NP

Heterogeneous excess argon and Neoproterozoic heating in the Usagaran Orogen, Tanzania, revealed by single grain $^{40}Ar/^{39}Ar$ thermochronology

Steven M. Reddy[1], Alan S. Collins[1*], Craig Buchan[1] and Abdul H. Mruma[2]

[1] *Tectonics Special Research Centre, Department of Applied Geology, Curtin University of Technology, PO Box U1987, Perth, WA 6845, Australia.*

2 Department of Geology, University of Dar-Es-Salaam, P.O.Box 35091, Dar-Es-Salaam, Tanzania

* *Present address: Dept. of Earth and Geographic Sciences, The University of Western Australia, Crawley, WA 6009, Australia.*

Short Title: Reddy et al; $^{40}Ar/^{39}Ar$ Dating of the Usagaran Orogen

Key Words: Palaeoproterozoic, Usagaran Orogen, East African Orogen, Ar laser microprobe, $^{40}Ar/^{39}Ar$ geochronology, deformation

Correspondence to Steve Reddy (e-mail: *S.Reddy@curtin.edu.au))*

Abstract

Existing tectonic models for the evolution of the Usagaran Orogen place strong significance on Palaeoproterozoic K-Ar and Rb-Sr ages. Laser $^{40}Ar/^{39}Ar$ data from single mica grains from the Isimani Suite near the western margin of the orogen indicate that excess ^{40}Ar is common in micas and this casts considerable doubt on tectonic models that are based on previously published K-Ar ages. Biotites lying within a well-developed S_2 foliation (previously constrained at 1999-1991 Ma) yield ages up to 3.3 Ga and contain a significant excess ^{40}Ar component that is variable at an intra- and inter sample scale. Textural evidence indicates that muscovite grew or recrystallised after the synkinematic biotites and they also record younger $^{40}Ar/^{39}Ar$ ages with individual steps from 524-1055 Ma. However, it is shown that the age difference does not reflect different periods of mica growth but the preferential partitioning of excess ^{40}Ar into the biotite. The muscovite data also have a component of excess ^{40}Ar and the youngest muscovite $^{40}Ar/^{39}Ar$ date (535.4 ± 2.3 Ma) indicates a maximum age for greenschist facies metamorphism. This date corresponds to thermal activity associated with the East African Orogen. Greenschist facies deformation (D_4 and D_5) is interpreted to have been coincident with this thermal event and indicates localised tectonic activity associated with Gondwanan amalgamation. The data are also consistent with greenschist facies deformation, metamorphism and deposition of the Usagaran Konse Group being of Neoproterozoic-Early Palaeozoic age. These new data therefore preclude a solely Palaeoproterozoic tectonic history for the Usagaran Orogen and indicate a complex thermal-tectonic reworking in the Neoproterozoic-Early Palaeozoic.

1. Introduction

The world's oldest known low-medium temperature subduction-related eclogites are found in the Usagaran Orogen of central Tanzania (Möller et al., 1995). The existence of these Palaeoproterozoic eclogites indicates the likelihood that subduction zone metamorphism was active as early as ~2.0 Ga and the Usagaran Orogen therefore provides an excellent opportunity to study "modern" plate tectonic processes in an ancient orogenic setting. An understanding of the thermal-tectonic evolution of the Usagaran Orogen has the potential to shed light on the thermal structure and tectonic evolution of Palaeoproterozoic subduction zone environments. It addition it may provide valuable constraints on the thermal evolution of the Earth and the geodynamic birth of "modern" plate tectonics.

Numerous studies have highlighted the Palaeoproterozoic history of the Usagaran Orogen (Wendt et al., 1972; Gabert, 1973; Gabert and Wendt, 1974; Reddy et al., 2003; Möller et al., 1995; Collins et al., 2004) and provided valuable constraints on the conditions and timing of high-pressure metamorphism. However, the Usagaran Orogen is bordered in eastern Tanzania by the East African Orogen, a Neoproterozoic to Cambrian orogenic belt thought to have developed at an active continental margin (Möller et al., 2000) and subsequent amalgamation of Gondwana by collision of the Indian Dharwar craton with East Africa (Stern, 1994; Dalziel, 1997). The structural and thermal significance of this collision event in modifying the existing Palaeoproterozoic architecture and thermal structure of the Usagaran Belt, although hinted at by several previous studies (Wendt et al., 1972; Möller et al., 1995), is far from clear. Yet discriminating the superimposed effects of the East African Orogen from older events is critical to correctly interpreting the Palaeoproterozoic evolution of the Usagran Orogen.

Reddy et al (2003) outlined a complex deformation history for the Isimani Suite exposed in the Great Ruaha river valley (Fig. 1) and subsequently placed constraints on the timing of high grade deformation and metamorphism (Collins et al., 2004). This study presents preliminary laser microprobe $^{40}Ar/^{39}Ar$ data from muscovites and biotite in an attempt to place temporal constraints on the lower grade parts of this deformation history. In so doing we assess both the potential problem of excess ^{40}Ar in Usagaran high-pressure metamorphic minerals and whether existing K-Ar data from the Usagaran Orogen (Wendt et al., 1972) could be affected by an excess ^{40}Ar component. The role of Neoproterozoic metamorphism and accompanying deformation associated with an East African Orogen overprint of the Usagaran Orogen is also addressed. Finally the mica data is used within a regional context to speculate on the stratigraphic age of Usagaran volcano-sedimentary cover sequences (the Konse Group) and is compared to data collected in previous studies from similar rocks of the Ubendian Orogen further west.

2. Geological Background and Geochronological Constraints

The Usagaran Orogen of central Tanzania is a Palaeoproterozoic orogenic belt that lies directly east of the Late Archaean Tanzanian craton (Fig. 1). It is subdivided into two major litho-tectonic units; the Konse Group and the Isimani Suite (Fig. 2). The Konse Group (Meinhold, 1970; Mruma, 1989), formerly the Konse Series (Whittingham, 1959; Harpum,

1970), comprises a stratigraphic succession of sedimentary and volcanic formations considered to have been deposited in the Palaeoproterozoic and subsequently metamorphosed at greenschist facies (Meinhold, 1970; Mruma, 1989) (Fig. 2). Locally the Konse Group lies uncomformably on deformed rocks of the Isimani Suite (Whittingham, 1959; Mruma, 1989), indicating its younger age. However, this contact is commonly reworked as a zone of younger localised deformation (Reddy et al., 2003).

The Isimani Suite (Mruma, 1989), previously referred to as the "Usagaran highly metamorphosed rocks" (Whittingham, 1959; Harpum, 1970) lies to the east of the Konse Group and comprises numerous different rock types that record a range of different metamorphic assemblages from eclogite (750-800°C and c.18kbar; Möller et al., 1995) through granulite-, amphibolite- and greenschist-facies (Mruma, 1989; Reddy et al., 2003). In part this range reflects variable degrees of retrograde synkinematic recrystallization (Reddy et al., 2003), but may also reflect varying metamorphic conditions within different parts of the suite.

Complex deformation within the Isimani Suite of the northern Usagaran Orogen can be described in terms of five events (Reddy et al., 2003). The most important of these (D_2) took place at amphibolite facies conditions and resulted in the accumulation of pervasive high strain deformation and mylonite formation throughout all of the exposed Isimani Suite in the Great Ruaha river section (Fig. 2). This D_2 deformation overprints high-pressure D_1 deformation and has been interpreted to reflect strain localisation and kinematic partitioning during sinistral transpression (Reddy et al., 2003). Younger greenschist facies shear zones with both extensional (D_4) and thrust (D_5) geometries cut the Isimani Suite, commonly marking the boundaries of D_2 structural domains, and also thrust the Isimani Suite over the Konse Group (Reddy et al., 2003).

Geochronological and isotopic data constrain the age of protolith formation, deformation and metamorphism within the Usagaran Orogen. Nd (T_{DM}) model ages of 2.5-3.1 Ga (Maboko and Nakamura, 1996; Möller et al., 1998; Maboko, 2000) and Pb-Pb feldspar data (Möller et al., 1998) indicate considerable Archaean material and little Palaeoproterozoic juvenile material within the Usagaran gneisses. Sensitive High Resolution Ion Microprobe (SHRIMP) U-Pb ages of 2705 ± 11 and 2698 ± 15 Ma from zircon cores, interpreted to date the timing of igneous crystallization of some of the Isimani protoliths also indicate the presence of Late

Archaean material (Reddy et al., 2003) and indicate a protolith that on temporal grounds appears similar to the Tanzanian craton (Maboko, 2000; Reddy et al., 2003).

Eclogite facies metamorphic conditions of 750°C and 18 kbar have been dated at c. 2000 Ma using $^{207}Pb/^{206}Pb$ monazite and titanite data (Möller et al., 1995) and more recently SHRIMP U-Pb zircon ages (Collins et al., 2004). An amphibolite facies overprint older than 1991± 2 Ma has been constrained by SHRIMP $^{207}Pb/^{206}Pb$ dating of zircons from a pegmatite that cuts high strain amphibolite facies fabrics (Collins et al., 2004). These data show that previously published younger Rb-Sr ages from Usagaran gneisses (e.g. Wendt et al., 1972) reflect disturbance of Sr after original crystallisation.

The Usagaran Orogen contains a series of post-tectonic granites, some of which have been dated by whole rock Rb/Sr and SHRIMP U/Pb zircon techniques. Post-kinematic granites in the Isimani Suite yield a whole-rock Rb/Sr age of 1845 ± 110 Ma (MSWD = 8.4, recalculated from Wendt et al. (1972) using the decay constant of (Steiger and Jager, 1977)) and a SHRIMP $^{207}Pb/^{206}Pb$ crystallization age of 1877 ± 7 Ma (Reddy et al.), while post-kinematic granites cutting the Ndembera Group yield a Rb/Sr date of 1787 ± 91 Ma (MSWD = 13, recalculated from Wendt et al. (1972) using the decay constant of Steiger and Jager (1977)). These data can be interpreted to indicate that the thermal-tectonic history for the Usagaran Orogen has been largely restricted to the Palaeoproterozoic. However, Rb-Sr and K-Ar data from biotite sampled from throughout the region span a range of ages with a minimum of *c.* 450 Ma (Wendt et al., 1972; Gabert and Wendt, 1974; Priem et al., 1979). Reworking of Tanzanian crust by the East African Orogen is dated in Tanzania at 610-655 Ma, (Möller et al., 2000; Muhungo et al., 2001) and the observed variation in biotite ages has been interpreted to reflect thermal resetting associated with the development of the East African Orogen to the east of the Usagaran Orogen (Fig. 1) (Wendt et al., 1972; Gabert, 1973; Priem et al., 1979). The thermal boundary recorded by these age variations has been used by previous workers to delineate the western margin of the East African Orogen in this region (Fig. 1) (Stern, 1994; Shackleton, 1996; Boven et al., 1999).

3. Sample Details and Analytical Procedure

Two orthogneiss samples (Fig. 2) from the Isimani Suite were selected from a sample suite collected while undertaking a structural transect along the Great Ruaha River (Reddy et al., 2003). Sample T01-19 (UTM 37S, 0184676E, 9209918S) is an intensely mylonitised gneiss

that preserves excellent top-to-the-NE δ-type kinematic indicators associated with D_2 amphibolite facies deformation (Reddy et al., 2003). Sample T01-24b (UTM 37S, 0182867E, 9210506S) is a granitic gneiss with a pronounced S_2 foliation and L_2 mineral elongation lineation defined by quartz and biotite. Both samples have mineral assemblages comprising plagioclase + orthoclase + quartz + biotite + muscovite + zoisite/epidote. In both samples biotites are aligned in the S_2 foliation and are well-preserved, showing no signs of alteration (Fig. 3a,c). The alignment of micas within the pervasive D_2 fabric indicates rotation or recrystallization of the grains during amphibolite facies metamorphic conditions that are independently constrained to 1991-1999 Ma (Collins et al., 2004). Muscovites from the samples are more complex. T01-19 muscovite appears to have locally overgrown biotite and is commonly highly oblique to the S_2 foliation (Fig. 3b). Minor epidote in the sample often rims biotite and is younger. Muscovites from T01-24b lie within the macroscopic S_2 foliation plane and show localised recrystallization to aggregates of finer grained muscovite that partly pseudomorph the primary muscovite grains (Fig. 3d).

Several grains of muscovite and biotite were handpicked from crushed whole rock samples of both T01-19 and T01-24b. Separated grains were cleaned in methanol and deionised water in an ultrasonic bath. Individual grains that showed no signs of being broken fragments of larger grains and showed no visible signs of alteration were selected for analysis. Multiple grain samples of each mica fraction were then individually wrapped in aluminium foil, and all the samples were loaded into an aluminium package. Biotite age standard Tinto B, with a K-Ar age of 409.24 ± 0.71 Ma was loaded at 5 mm intervals along the package to monitor the neutron flux gradient. The package was Cd-shielded and irradiated in the H5 position of the McMaster University Nuclear Reactor, Hamilton, Canada, for 90 hours.

Argon analyses were undertaken at the Western Australian Argon Isotope Facility, Curtin University of Technology, operated by a consortium consisting of Curtin University and the University of Western Australia. Argon data were collected by infra-red laser step-heating of single grains. Irradiated mineral samples were loaded into an ultra-high vacuum laser chamber with a Kovar viewport and baked to 120°C overnight to remove adsorbed atmospheric argon from the samples and chamber walls. A 110 W Spectron Laser Systems continuous-wave neodymium-yttrium-aluminium-garnet (CW-Nd-YAG) laser (λ = 1064 nm), fitted with a TEM00 aperture, was used to laser step-heat the mineral sample at increasing laser power (9.9-10.1A). The laser was fired through a Merchantek computer-controlled X-Y-

Z sample chamber stage and microscope system, fitted with a high-resolution CCD camera, 6x computer controlled zoom, high magnification objective lens, and two light sources for sample illumination. Prior to analysis, the dimensions of each grain were measured using the calibrated stage system.

The gases released by laser heating were gettered using 3 SAES AP10 getter pumps to remove all active gases (CO_2, H_2O, H_2, N_2, O_2, CH_4). The remaining noble gases were equilibrated into a high sensitivity mass spectrometer (MAP 215-50), operated at a mass-resolution of 600, and fitted with a Balzers SEV 217 multiplier. The automated extraction and data acquisition system was computer controlled, using a LabView program. Mean 5 minute extraction system blanks obtained during data collection were 4.6×10^{-12}, 7.7×10^{-15}, 5×10^{-15}, 1.1×10^{-13}, and 3×10^{-14} cm^3 at standard temperature and pressure for ^{40}Ar, ^{39}Ar, ^{38}Ar, ^{37}Ar, and ^{36}Ar respectively. Data were corrected for mass spectrometer discrimination and nuclear interference reactions. $^{40}Ar/^{39}Ar$ ages were calculated using the decay constant quoted by Steiger and Jäger (1977). J values and 1σ errors are noted in Table 1. Errors shown in step-heating profiles (Fig. 4) represent analytical errors and do not include J value uncertainties.

4. $^{40}Ar/^{39}Ar$ Results

Muscovite and biotite argon data from two samples less than 2km apart (Fig. 2) are reported in Table 1 and plotted with respect to cumulative ^{39}Ar% in Fig. 4. For each sample, age (calculated from $^{40}Ar/^{39}Ar$), $^{37}Ar/^{39}Ar$ and $^{38}Ar/^{39}Ar$ are plotted for each sample. The latter two ratios are related to Ca/K and Cl/K ratios respectively (McDougall and Harrison, 1999). Each step-heating profile represents the analysis of a single mica grain.

Biotite data from individual grains of T01-19 yield relatively flat apparent age profiles with individual step ages increasing with cumulative ^{39}Ar% (Fig. 4a). However apparent ages from different single grains vary by up to 160 Ma and range from *c.* 1370-1530 Ma. This variation does not correlate with measured grain diameters (Fig. 4a). None of the grains yield statistically valid plateaux. However, if J value errors (Table 1) are included in the plateaux calculations, then grain 2 yields a plateau age of 1383.9 ± 2.4 Ma (1σ) and grain 3 gives a plateau age of 1529 ± 3 Ma (1σ). These plateaux include all but step 1 and 92.3% of ^{39}Ar (MSWD = 0.58) for grain 2 and 100% of the ^{39}Ar of grain 3 (MSWD = 2.1). $^{38}Ar/^{39}Ar$ data from the same grains are low and show flat spectra of *c*. 0.014 and indicate little variation in Cl both within grains and between grains (Fig. 4a). Small values of $^{37}Ar/^{39}Ar$ (Fig. 4a)

indicate no significant contamination by Ca-bearing phases. In most cases the $^{37}Ar/^{39}Ar$ step pattern mirrors that shown by the age spectra. However, the first step, which correlates with lower apparent age, always yields a higher $^{37}Ar/^{39}Ar$ ratio than the second step. This appears to indicate a small compositional control on the first step and a very minor component of lower apparent age material within the biotite grain.

A similar pattern of within-grain apparent ages profiles is seen in biotite grains from T01-24b (Fig. 4c). However, individual grains yield significantly older apparent ages than T01-19 biotites, ranging from *c.* 3200-3740 Ma (Fig. 4c). Again, individual grains yield different ages (Fig. 4c). No plateaux were obtained when J value errors were excluded from the plateaux calculations. However, including J value uncertainty gave a plateau (steps 3-6) for grain 2 of 3728.2 ± 4.3 Ma (1σ), which includes 58.8% of the ^{39}Ar and an MSWD of 0.56. In both analysed grains the first step yields ages younger than subsequent steps. Values for $^{37}Ar/^{39}Ar$ and $^{38}Ar/^{39}Ar$ are low (Fig. 4c) and are similar to those in T01-19 biotites. However, the relationship between apparent age and both $^{37}Ar/^{39}Ar$ and $^{38}Ar/^{39}Ar$ are complex. This complexity is seen in the relationship of apparent age highs and lows with corresponding steps in the $^{37}Ar/^{39}Ar$ and $^{38}Ar/^{39}Ar$ profiles. In some cases (e.g. grain 1, step 5) apparent age lows correspond to highs in both $^{37}Ar/^{39}Ar$ and $^{38}Ar/^{39}Ar$ (Fig. 4c). In grain 2 (step 3) an apparent age high correlates with a high in $^{37}Ar/^{39}Ar$ and a low in $^{38}Ar/^{39}Ar$ (Fig. 4c). An apparent age low corresponds to a low in $^{37}Ar/^{39}Ar$ and a high in $^{38}Ar/^{39}Ar$ in grain 1, step 1 (Fig. 4c). These relationships indicate that a number of factors affect the range in apparent ages obtained from single grains. However, it should be noted that the values of $^{37}Ar/^{39}Ar$ and $^{38}Ar/^{39}Ar$ are small, as are within-grain variations with respect to 2σ errors, indicating no significant contamination by Ca-bearing phases and little Cl variability associated with heterogeneous alteration.

Muscovite grains from T01-19 yield ages ranging from *c.* 524 -728 Ma (Table 1). The data form relatively flat spectra with grain 1 giving older apparent ages in the last few steps of the profile (Fig. 4b). Although the profiles are relatively flat, grain 2 only yields a plateau if J value errors are included in the plateau calculation. The plateau age of 535.4 ± 1.2 Ma (1σ) includes 4 steps incorporating 63.6% of the ^{39}Ar (MSWD = 0.39) and is significantly younger than biotite ages from the same sample (Fig. 4a). Again the ages of the two different mica grains differ by c. 100 Ma despite a similar grain diameter of 300μm (Fig. 4b). $^{38}Ar/^{39}Ar$ data from muscovite are relatively homogenous and similar for both grains. However, $^{37}Ar/^{39}Ar$

data from the two grains are very different with grain 1 having values an order of magnitude greater than other micas analysed in this study (Fig. 4).

Apparent ages from muscovite grains from T01-24b range from 832 – 1055 Ma (Table 1). Age spectra indicate some variability and the data yield no plateaux even if J value uncertainties are taken into account. The spectra show that earlier steps yield older apparent ages than steps released later in the heating cycle (Fig. 4d). However all apparent ages from T01-24b muscovite are higher than muscovite ages from T01-19 (cf. Figs 4b,d). $^{38}Ar/^{39}Ar$ data from the muscovite have similar values to other mica analyses (*c*. 0.013) and are relatively homogenous, though increasing slightly with increasing $^{39}Ar\%$. $^{37}Ar/^{39}Ar$ data from the two grains differ with respect to the apparent age profiles. In grain 2 the profiles for apparent age and $^{37}Ar/^{39}Ar$ are complimentary and follow the same decreasing pattern at increasing $^{39}Ar\%$. However, grain 1 generally shows lower values than grain 2 and apparent age highs and lows correspond to $^{37}Ar/^{39}Ar$ lows and highs respectively. It must be noted though that if 2σ errors are considered then the $^{37}Ar/^{39}Ar$ ratios for each step within individual grains are within error and the significance of similarity in apparent ages and $^{37}Ar/^{39}Ar$ profiles is difficult to confirm.

All mica analyses have negligible ^{36}Ar, indicating that there is no atmospheric ^{40}Ar component in the samples and also precluding the use of inverse isochron ($^{39}Ar/^{40}Ar$ vs $^{36}Ar/^{40}Ar$) plots to recognise any excess ^{40}Ar component.

5. Discussion

5.1 Interpretation of the Ar data

The Ar data show complexity that cannot be explained by simple closure temperature models for Ar diffusion in micas. The $^{40}Ar/^{39}Ar$ data record a wide range of apparent ages with biotite from both samples being older than corresponding muscovite ages. This is inconsistent with higher closure temperature estimates for Ar diffusion in muscovite than biotite for the similar grain sizes analysed here (Villa, 1997; McDougall and Harrison, 1999). In addition, age variations amongst single grains from individual samples show no correlation with measured grain diameter (Fig. 4). The closure temperature model therefore fails to account for such variations and within-sample heterogeneity in Ar isotope systematics at the grain scale is required.

The age variation amongst biotite single grain data from both samples does not seem to reflect primary compositional variations or secondary alteration that can be inferred from the distribution of ^{38}Ar and ^{37}Ar isotopes. However, the correlation of slightly increased $^{37}Ar/^{39}Ar$ with lower apparent ages in the first steps of T01-19 biotite analyses may reflect minor contamination by a component with a slightly higher $^{37}Ar/^{39}Ar$ ratio and younger apparent age, for example muscovite (Fig. 4b). The correlation of younger age with slightly increased $^{38}Ar/^{39}Ar$ ratios in T01-24b biotites may indicate slight alteration and Ar loss from the least retentive sites of the lattice. However, all of these variations are minor and cannot account for the observed range of ages.

The $^{40}Ar/^{39}Ar$ ages from T01-24b biotite are significantly older than the ~2.7 Ga igneous protolith age of Isimani gneiss (Reddy et al., 2003) and are also older than the 1991-1999 Ma age of syn-D_2 amphibolite facies fabrics (Collins et al., 2004) in which the analysed micas lie. These data are therefore interpreted to reflect the presence of an excess ^{40}Ar component within the biotite. The observation of increased age with smaller grain diameter is consistent with such an interpretation if the excess ^{40}Ar component was added to the grain by a diffusive process after grain growth rather than being incorporated into the grain during original growth (Reddy et al., 1996).

Biotite data from T01-19 are more difficult to interpret because they yield ages that are younger than the inferred age of the D_2 fabrics. The ages could therefore reflect cooling from *c.* 2 Ga amphibolite facies metamorphism. However an alternative interpretation is that the ages could still reflect a component of excess ^{40}Ar added to the biotite since original cooling from this 2 Ga event. In this case the difference in ages between single grain analyses may reflect the heterogeneous distribution of an excess ^{40}Ar component in the rock and the ability of grains to be affected by this component (Reddy et al., 1996; Reddy et al., 1997).

Muscovite from both T01-19 and T01-24b yield Neoproterozoic ages that are significantly younger than the Palaeoproterozoic eclogite and amphibolite metamorphic ages for the Isimani Suite (Möller et al., 1995; Collins et al., 2004). Muscovite apparent ages from T01-19 are significantly younger than apparent ages from T01-24b – a pattern that mimics the apparent age distribution of the biotite data.

T01-24b muscovites lie within the S_2 foliation, are interpreted to have grown or recrystallised at the same time as the foliation (*c*. 2 Ga) and have been subsequently recrystallised to finer

grained aggregates of muscovite (Fig. 3d). Ar data from T01-24b muscovite indicate that, within error limits, there is little compositional control on apparent age and lower retentivity sites correlate with slightly increased apparent ages. In addition the slightly smaller of the two analysed grains yields slightly higher apparent ages. However, the measured grain size may be misleading because we were unable to assess the extent of recrystallization in the analysed grains. Two possible interpretations of the 900 Ma age are that it represents the time that the muscovites passed through their closure temperature or the time of coarse muscovite recrystallization to fine aggregates. The data from T01-19 preclude the first of these interpretations because the coarser grain size of T01-19 muscovite would require the finer grain size of T01-24 to yield ages <535 Ma. In the second interpretation the recrystallization age would only be preserved if the recrystallization temperature was less than the closure temperature of the recrystallised muscovite (Reddy and Potts, 1999). Since data from T01-19 indicates that the closure temperature for coarser muscovite was much younger than 900 Ma, this age cannot correspond to the timing of recrystallization.

Earlier it was suggested that >3.3 Ga biotite ages from T01-24 were related to heterogeneous excess ^{40}Ar and have no geological significance. Biotite tends to have a greater affinity for excess ^{40}Ar than muscovite (Roddick et al., 1980; Dahl, 1996), but the presence of excess ^{40}Ar in biotite indicates that muscovite may also be affected by a smaller excess ^{40}Ar component. Muscovite data from T01-24b cannot be reconciled with closure temperature or recrystallization models. However, the fact that ages are *c.* 400 Ma older than nearby muscovites of T01-19 demonstrates that the muscovites of T01-24 are probably affected by excess ^{40}Ar.

A correlation of increased muscovite age with order of magnitude increase in $^{37}Ar/^{39}Ar$ in T01-19 is interpreted to reflect minor contamination by a Ca bearing phase of older apparent age. This indicates that the younger age of 535.4 ± 1.2 Ma (1σ) is the most reliable muscovite age. Since muscovites in T01-19 overprint biotite and lie oblique to the S_2 foliation (Fig. 3b), indicating that they post-date biotite growth, the age of 535 Ma may reflect either the timing of this muscovite growth and metamorphism, if the temperature conditions of growth were lower than the closure temperature, or the time at which the muscovite passed through it's closure temperature after growth. For the first interpretation to be correct, the muscovite would need to have grown at temperatures below its closure temperature (*c.* 350°C). The metamorphic conditions of muscovite growth are difficult to constrain. However, given the

occurrence of both muscovite and epidote and the resetting of monazite U-Pb ages (Möller et al., 1995), we suggest greenschist facies conditions with temperatures higher than the muscovite closure temperature. It is therefore more likely that the age reflects isotopic modification after growth.

The diffusion parameters for Ar diffusion in biotite and muscovite are such that Ar diffusion in biotite should be faster than in muscovite in grains of the same grain size within the same sample (e.g. (McDougall and Harrison, 1999). This is reflected in the lower closure temperature of biotite for Ar diffusion and it would be expected that 300μm biotite grains from T01-19 would record lower ages than muscovite of the same grain size. This is not so and older biotite ages are interpreted to reflect the preferred partitioning of excess ^{40}Ar into biotite (Roddick et al., 1980; Dahl, 1996). The presence of excess ^{40}Ar in biotite indicates the plateau age of 535.4 Ma from T01-19 may also be artificially high due to an excess ^{40}Ar component. Therefore, the age of 535.4 Ma must be interpreted to be a maximum age for closure of the muscovite to Ar diffusion, noting that if it did contain an excess ^{40}Ar component that the timing of isotopic closure would be younger.

The differences in ages amongst individual grains from the same samples are not easily explained by the available data. However, such variations are commonly observed in detailed studies of intragrain microstructure and argon isotope systematics (e.g. Reddy et al., 1996; Reddy et al., 2001). From such studies it is clear that the internal microstructure of individual grains can vary markedly within individual samples and this variation can lead to significant age variations between grains. In part this reflects the heterogeneous reduction in effective diffusion distances and diffusion pathways within grains. In this study we have not undertaken a detailed microstructural analysis of the actual grains analysed for Ar. However this work is currently ongoing.

In summary, the preferred interpretation is that the Mesoproterozoic ages recorded by T01-19 and T01-24b biotites reflect the incorporation of an excess ^{40}Ar component. The different ages recorded by different grains from each sample reflects a heterogeneous distribution of excess ^{40}Ar within different grains. The best estimate of the timing of the addition of the excess ^{40}Ar to both samples is around the time recorded by the least affected muscovite grain, that is around 535 Ma. This date may reflect a maximum age for a period of muscovite growth or, more likely, a maximum age for muscovite cooling through its closure

temperature. In either case the data indicate a significant thermal event associated with the East African Orogen.

5.2 Relationship of $^{40}Ar/^{39}Ar$ ages to previous studies

Previous mineral age data collected from the southern Usagaran Orogen has been used to argue for a progressive overprint of Usagaran micas by a Palaeozoic heating event (Wendt et al., 1972). The basis for this interpretation was the range of Palaeoproterozoic to Palaeozoic Rb-Sr and K-Ar ages (Wendt et al., 1972). However, the original data of Wendt is difficult to reconcile with a simple Palaeoproterozoic cooling history followed by a localised thermal event for several reasons.

Firstly, several of the samples yield K/Ar ages that are older than the protolith age and were interpreted as being affected by excess ^{40}Ar (Wendt et al., 1972). The distribution of these samples and a further 8 dated samples, is not shown in Wendt et al's (1972) location map, therefore we are unable to comment on the spatial distribution of excess ^{40}Ar ages. However, it is unlikely that all samples affected by excess ^{40}Ar will yield ages older than the protolith ages and dates younger than the protolith age may also contain an excess ^{40}Ar component. Indeed, although acknowledging that our data come from samples from a different area, we argue that the data from T01-19 indicates that biotites yielding Mesoproterozoic ages are affected by an excess ^{40}Ar component.

Secondly, the distribution of biotite K-Ar and Rb-Sr ages are often discordant (Wendt et al., 1972) when they should be similar because of the diffusion characteristics of the two isotope systems. It is difficult to assess the reason for this from the original data. However in the most extreme example, biotites yielding 479 Ma Rb-Sr ages give K-Ar ages >2700 Ma. In this case excess ^{40}Ar affecting the K-Ar date is the most likely interpretation. In addition, the method by which Wendt et al (1972) estimated initial $^{87}Sr/^{86}Sr$ ratios for mineral ages is unclear but could be a source of error in the Rb/Sr mica age.

The spatial distribution of Rb/Sr and K/Ar variations seems to follow a NE-SW trend (Wendt et al., 1972) similar to the orientation of structures in the East African Orogen further east. This similarity in orientation has been used to argue for resetting of radiometric ages during this orogenic event (Wendt et al., 1972). However, the variation in K/Ar ages has similarities to the spatial distribution of rock types in the Usagaran Orogen, with younger ages correlating with the location of Isimani Suite migmatities (Gabert, 1973). These migmatites have much

lower K contents than Usagaran granites (Gabert, 1973) that yield the older K/Ar ages. Since the amount of locally derived excess ^{40}Ar will reflect the bulk-rock K content of the rock (Reddy et al., 1997), the distribution of apparent K-Ar ages is therefore consistent with incorporation of heterogeneous excess ^{40}Ar derived by degassing of local K-rich phases.

The 535 Ma muscovite age from T01-19 indicates that at least parts of the Isimani Suite were at temperatures above the closure temperature for muscovite (350-400°C), and thus biotite, in the Early Palaeozoic. The data presented, combined with the wide range in K-Ar ages and the published discordance between Rb/Sr and K/Ar ages, are consistent with the thermal opening of micas to isotopic diffusion during the early Palaeozoic and the heterogeneous diffusion of excess ^{40}Ar into mica. The range of Palaeoproterozoic to Palaeozoic ages do not therefore represent the timing of cooling below the biotite closure temperature, or simple thermal resetting but the heterogeneous distribution of excess ^{40}Ar during Palaeozoic heating at greenschist facies conditions.

To the south and west, the Usagaran Orogen links with the similar Ubendian Orogen of western Tanzania. These two orogenic belts are considered by many to be equivalent (Meinhold, 1970; Gabert and Wendt, 1974; Priem et al., 1979; Lenoir et al., 1994). Recent geochronological data support the similar metamorphic histories of the two belts with high pressure granulite-eclogite facies metamorphism at c. 2000 Ma (Möller et al., 1995; Ring et al., 1997; Collins et al., 2004) overprinted by younger amphibolite facies metamorphism at <1991 Ma in the Usagaran Orogen (Collins et al., 2004) and younger than 1860 Ma in the Ubende belt (Lenoir et al., 1994). $^{40}Ar/^{39}Ar$ data from the Ubendian Orogen are limited to barroisite analyses. These data are difficult to interpret and individual release spectra range over from Palaeozoic to Palaeoproterozoic in age (Boven et al., 1999). Despite this complexity, Boven et al (1999) interpret an age of 1848 ± 6 Ma to reflect cooling through the amphibole closure temperature (500-550°C) with older ages reflecting a component of excess ^{40}Ar and younger ages reflecting alteration and ^{40}Ar loss. These data were interpreted to show that exhumation of the Ubendian high-pressure metamorphic rocks took place in the Palaeoproterozoic with little subsequent thermal activity (Boven et al., 1999). A similar range of ages and complexity to the Ubende Ar data is shown by the mica data presented here. However our interpretation differs significantly from that of Boven et al (1999). Clearly resolution of the Palaeoproterozoic cooling of these high pressure rocks and any subsequent reheating associated with the East African Orogen requires further studies at a regional scale.

5.3 Relationship of $^{40}Ar/^{39}Ar$ ages to structural and stratigraphic models

Easterly dipping shear zones are found at various structural levels within the Isimani Suite of the Usargaran Orogen (D_4 and D_5 of Reddy et al., 2003). These record both W-directed thrust and E-directed extensional displacements and clearly overprint peak metamorphic assemblages. Both kinematic types of shear zone preserve microstructures and mineral assemblages that suggest deformation took place at greenschist facies conditions. The kinematic framework of these structures contrasts that preserved in amphibolite grade structures (Reddy et al., 2003) but have similar geometries and kinematics to structures in the nearby East African Orogen. $^{40}Ar/^{39}Ar$ data demonstrates that the Isimani Suite was at greenschist facies temperatures in Early Palaeozoic times and given the absence of annealing of D_4 and D_5 structures it is interpreted that they formed in late Neoproterozoic-Early Palaeozoic times towards the western margin of the East African Orogen.

The metasedimentary and metavolcanic Konse Group is thought to have been deposited and metamorphosed in the Palaeoproterozoic (Meinhold, 1970; Whittingham, 1959; Mruma, 1989). Greenschist facies metamorphism in the Konse Group was previously thought to have developed simultaneously with the main deformation phase in the Isimani Suite (Mruma 1989). However where undisturbed, the Konse Group unconformably overlies foliated rocks of the Tanzanian Craton and the Isimani Suite (Whittingham, 1959; Mruma, 1989) and therefore must represent a volcano-sedimentary sequence formed after exhumation of the Isimani Suite. In the area studied here, the contact between the Isimani Suite and Konse Group is a greenschist facies high strain zone (D_5), the Ifwambo Thrust of Mruma (1989), which accommodates westward thrusting of the higher grade Isimani Suite onto the Konse Group (Reddy et al., 2003). Kinematic data (Reddy et al., 2003) and the $^{40}Ar/^{39}Ar$ data presented here indicate that this deformation was probably associated with the East African Orogeny. It is therefore possible that the greenschist facies metamorphism and deformation of the structurally lower Konse Group reflects heating and more pervasive deformation in the footwall of the Ifwambo Thrust at the same time as East African Orogeny crustal thickening.

If it is correct that Konse Group deformation and metamorphism developed during the Neoproterozoic-Early Palaeozoic East African Orogeny rather than the Palaeoproterozoic Usagaran Orogeny, then the age of the Konse Group deposition is also questionable. The Palaeoproterozoic depositional age of the Konse Group is only independently supported by correlation of the Konse Group with a sequence of rocks known as the Ndembera Volcanics

(Whittingham, 1959; Mruma, 1989). These rocks have been dated using Rb-Sr and yield depositional ages of 1895 ± 27 Ma (age recalculated from Wendt et al (1972) using the decay constant of Steiger and Jager (1977)). If these volcanics can be linked directly to the Konse Group volcanics or if the Ndembera Volcanics clearly post-date the Konse Group then the Palaeoproterozoic depositional age of the Konse Group is confirmed. However, the correlation and relationship between the two units is far from clear. At this stage there is no evidence to support the Palaeoproterozoic depositional age of the Konse Group and, given the likelihood that its metamorphic overprint reflects Neoproterozoic-Early Palaeozoic tectonism, it can be speculated that the volcano-sedimentary sequence may be much younger than previously thought. Clearly further detailed geochronological work is required to further test these ideas.

6. Conclusions

The main conclusions of this study are:

1) $^{40}Ar/^{39}Ar$ single grain data from biotites and muscovites taken from orthogneisses of the Isimani Suite within the Palaeoproterozoic Usagaran Orogen demonstrate complex Ar isotope systematics due to isotopic remobilisation and incorporation of excess ^{40}Ar.
2) Textural evidence that muscovite growth postdates biotite growth does not explain the observed age difference between the older biotite and younger muscovite data. Instead it reflects the heterogeneous partitioning of excess ^{40}Ar preferentially into the biotite.
3) The youngest reliable muscovite age of 535 Ma is a maximum age for cooling of the samples through the muscovite closure temperature and indicates that the thermal event responsible for Ar migration was associated with the Neoproterozoic – Early Palaeozoic East African Orogen.
4) Greenschist facies shear zones that cut the Isimani Suite (D_4 and D_5 of Reddy et al, 2003) are interpreted to have formed during a Neoproterozoic – Early Palaeozoic event associated with the East African Orogen. The Ar data are consistent with pervasive greenschist-facies metamorphism, deformation and deposition of the Konse Group also having taken place at this time.
5) These new data preclude a solely Palaeoproterozoic tectonic history for the Usagaran Orogen and indicate a complex thermal-tectonic reworking in the Neoproterozoic-Early Palaeozoic that is more significant than previously thought.

Acknowledgements

This work was funded by Australian Research Council grants to SMR, ASC and ACB. Jo-Anne Wartho is thanked for assistance in the Ar lab. Ken Ludwig (Berkeley) is thanked for supplying his programme Isoplot 2.49. Andreas Möller and Jean-Paul Liégeois are thanked for critical reviews of the manuscript. This paper is Tectonics Special Research Centre Publication No. 238.

References

Boven, A., Theunissen, K., Sklyarov, E., Klerkx, J., Melnikov, A., Mruma, A. and Punzalan, L., 1999. Timing of exhumation of a high pressure mafic granulite terrane of the Palaeoproterozoic Ubende belt (west Tanzania). Precambrian Research, 93: 119-137.

Collins, A.S., Reddy, S.M., Buchan, A.C. and Mruma, A.H., 2004. Temporal constraints on Palaeoproterozoic eclogite formation and exhumation. Earth and Planetary Science Letters, In Press.

Dahl, P.S., 1996. The crystal-chemical basis for Ar retention in micas - inferences from interlayer partitioning and implications for geochronology. Contributions to Mineralogy and Petrology, 123(1): 22-39.

Dalziel, I.W.D., 1997. Neoproterozoic-Paleozoic geography and tectonics: Review, hypothesis, environmental speculation. Geological Society of America Bulletin, 109: 16-42.

Gabert, G., 1973. Uber präambrische Olivinmonzoite (Kentallenite) in Zentral-Tanzania. Geologische Jahrbuch, B6: 51-79.

Gabert, G. and Wendt, I., 1974. Datierung von granitische Gesteine im Dodoman- und Usagaran-System und in der Ndembera-Serie (Tanzania). Geologische Jahrbuch, B11: 3-55.

Harpum, J.R., 1970. Summary of the Geology of Tanzania, Part V: Structure and Geotectonics of the Precambrian, Resources Division, Dodoma, Tanzania.

Lenoir, J.-L., Liégeois, J.-P., Theunissen, K. and Klerkx, J., 1994. The Palaeoproterozoic Ubendian shear belt in Tanzania: geochronology and structure. Journal Of African Earth Sciences, 19: 169-184.

Maboko, M.A.H., 2000. Nd and Sr isotopic investigation of the Archean-Proterozoic boundary in north eastern Tanzania: constraints on the nature of Neoproterozoic tectonism in the Mozambique Belt. Precambrian Research, 102: 87-98.

Maboko, M.A.H. and Nakamura, E., 1996. Nd and Sr isotopic maping of the Archaean-Proterozoic boundaru in southeastern Tanzania using granites as probes for crustal growth. Precambrian Research, 107: 105-115.

McDougall, I. and Harrison, T.M., 1999. Geochronology and thermochronology by the $^{40}Ar/^{39}Ar$ method. Oxford University Press, Oxford, UK, 269 pp.

Meinhold, K.D., 1970. Petrographie, Metamorphose, Tektonik und Stratigraphische Stellung der Konse-Series in Zentral-Tanzania (Ostafrika). Geologische Jahrbuch, 91, 137 pp.

Möller, A., Appel, P., Mezger, K. and Schenk, V., 1995. Evidence for a 2Ga subduction zone: eclogites in the Usagarian belt of Tanzania. Geology, 23: 1067-1070.

Möller, A., Mezger, K. and Schenk, V., 1998. Crustal age domains and the evolution of the continental crust in the Mozambique Belt of Tanzania: Combined Sm-Nd, Rb-Sr, and Pb-Pb Isotopic Evidence. Journal of Petrology, 39: 749-783.

Möller, A., Mezger, K. and Schenk, V., 2000. U-Pb dating of metamorphic minerals: Pan-African metamorphism and prolonged slow cooling of high pressure granulites in Tanzania, East Africa. Precambrian Research, 104: 123-146.

Mruma, A.H., 1989. Stratigraphy, metamorphism and tectonic evolution of the Early Proterozoic Usagaran Belt, Tanzania. Res Terrae, Ser. A., No. 2: 203.

Muhungo, S., Kröner, A. and Nemechin, A.A., 2001. Single zircon evaporation and SHRIMP ages for granulite-facies rocks in the Mozambique Belt of Tanzania. Journal of Geology, 109: 171-189.

Priem, H.N.A., Boelrijk, N.A.I.M., Hebeda, E.H., Verdurmen, E.A.T., Verschure, R.H., Oen, I.S. and Westra, L., 1979. Isotopic age determinations on granitic and gneissic rocks from the Ubendian-Usagaran system in southern Tanzania. Precambrian Research, 9: 227-239.

Reddy, S.M., Collins, A.S. and Mruma, A., 2003. Complex high-strain deformation in the Usagaran Orogen, Tanzania: structural setting of Palaeoproterozoic eclogites. Tectonophysics, 375: 101-123.

Reddy, S.M., Kelley, S.P. and Magennis, L., 1997. A microstructural and argon laserprobe study of shear zone development on the western margin of the Nanga Parbat Syntaxis, north Pakistan. Contributions to Mineralogy and Petrology, 128: 16-29.

Reddy, S.M., Kelley, S.P. and Wheeler, J., 1996. A $^{40}Ar/^{39}Ar$ laserprobe study of rocks from the Sesia Zone: Excess argon, argon loss and implications for metamorphic and deformation histories. Journal of Metamorphic Geology, 14: 493-508.

Reddy, S.M., Potts, G.J. and Kelley, S.P. 2001. $^{40}Ar/^{39}Ar$ ages in deformed potassum feldspar: evidence of microstructural control on Ar isotope systematics. Contributions to Mineralogy and Petrology, 141: 186-200.

Reddy, S.M. and Potts, G.J., 1999. Constraining absolute deformation ages: The relationship between deformation mechanisms and isotope systematics. Journal of Structural Geology, 21: 1255-1265.

Ring, U., Kröner, A. and Toulkeridis, T., 1997. Palaeoproterozoic granulite-facies metamorphism and granitiod intrusions in the Ubendian-Usagaran Orogen of northern Malawi, east-central Africa. Precambrian Research, 85: 27-51.

Roddick, J.C., Cliff, R.A. and Rex, D.C., 1980. The evolution of excess argon in Alpine biotites - a ^{40}Ar-^{39}Ar analysis. Earth and Planetary Science Letters, 48: 185-208.

Shackleton, R.M., 1996. The final collision between East and West Gondwana; where is it? Journal of African Earth Sciences, 23: 271-287.

Steiger, R.H. and Jager, E., 1977. Subcommision on Geochronology: Convention on the use of decay constants in geo- and cosmochronology. Earth and Planetary Science Letters, 36: 359-362.

Stern, R.J., 1994. Arc Assembly and continental collision in the Neoproterozoic East African orogeny - implications for the consolidation of Gondwana. Annual Review of Earth and Planetary Sciences, 22: 319-351.

Villa, I.M., 1997. Isotopic closure. Terra Nova, 10: 42-47.

Wendt, I., Besang, C., Harre, W., Kreuzer, H., Lenz, H. and Müller, P., 1972. Age determinations of granitic intrusions and metamorphic events in the early Precambrian of Tanzania, 24th International Geological Congress, Montreal, Section 1, pp. 295-314.

Whittingham, J.K., 1959. The Geology of the Nyanzwa area. Bulletin of the Geological Survey of Tanganyika, pp. 27.

Table Captions

Table 1: Ar isotopic data obtained by infra-red single grain laser step-heating of muscovites and biotites from orthogneiss samples T01-19 and T01-24b from the Isimani Suite, Usagaran Orogen. See Fig. 2 for sample locations.

Figure Captions

Figure 1: Location of the Usagaran Orogen and its relationship to the EAO and the Ubendian Orogen. The box marks the boundaries of Fig. 2. L. Tan = Lake Tanganyika.

Figure 2: Geological map of part of the Usagaran Orogen, Tanzania. Map and lithological subdivisions are after Mruma (1989) and Whittingham (1959). Ifwambo = Ifwambo Thrust, identified and named in Mruma (1989). Yalumba Hill, contains well preserved eclogite-facies assemblages (Möller, 1995).

Figure 3: Photomicrographs showing micas from samples T01-19 and T01-24b. a) Biotite (b) from T0/19 showing alignment of basal (001) cleavage parallel to S_2 foliation and no visible alteration. b) T0/19 muscovite (m) at high angles to S_2 and overgrowing biotite. c) T01-24b biotite (b) showing alignment of basal (001) cleavage parallel to S_2 foliation. d) Muscovite (m) from T01-24b showing recrystallisation to finer aggregates of muscovite.

Figure 4: Ar laser step heating profiles on single grains. a) Three biotite grains from T01-19; b); Two muscovite grains from T01-19; c) Two biotite grains from T01-24b; d) Two muscovite grains from T01-24b. Data are presented in Table 1.

Sample	$^{40}Ar/^{39}Ar$	+-	$^{38}Ar/^{39}Ar$	+-	$^{37}Ar/^{39}Ar$	+-	$^{36}Ar/^{39}Ar$	+-	^{39}Ar (cm^3)	+-	Cumulative % ^{39}Ar	Atmos. Ar %	$^{40}Ar^*/^{39}Ar$	+-	Age (Ma)	+- (1σ)
T01-19 biotite: J value = 0.018579 ± 0.000093																
T01-19 bte grain 1.1	69.022	0.043	0.01439	0.00001	0.00346	0.00085	0.00104	-	1.30E-11	8.13E-15	64.2	0.44	68.715	0.043	**1484**	**5**
T01-19 bte grain 1.2	70.019	0.058	0.01496	0.00001	-	-	0.00121	-	6.73E-12	5.42E-15	97.4	0.51	69.662	0.058	**1498**	**5**
T01-19 bte grain 1.3	67.665	0.120	0.00535	0.00000	-	-	-	-	5.23E-13	0.00E+00	100.0	0.00	67.665	0.120	**1469**	**5**
T01-19 bte grain 2.1	63.366	0.050	0.01409	0.00001	0.00429	0.00000	0.00798	0.00001	1.05E-11	8.13E-15	7.7	3.72	61.008	0.048	**1367**	**5**
T01-19 bte grain 2.2	62.296	0.026	0.01307	0.00006	0.00274	0.00021	0.00131	0.00005	5.37E-11	2.17E-14	46.9	0.62	61.908	0.030	**1381**	**5**
T01-19 bte grain 2.3	62.171	0.016	0.01311	0.00008	0.00345	0.00044	0.00053	0.00008	3.60E-11	5.59E-15	73.3	0.25	62.015	0.027	**1383**	**5**
T01-19 bte grain 2.4	61.990	0.006	0.01322	0.00016	0.00205	0.00000	-	-	1.65E-11	0.00E+00	85.3	0.00	61.990	0.006	**1382**	**5**
T01-19 bte grain 2.5	62.597	0.026	0.01326	0.00001	0.00564	0.00056	0.00054	-	2.00E-11	8.13E-15	100.0	0.25	62.438	0.026	**1389**	**5**
T01-19 bte grain 3.1	72.772	0.026	0.01462	0.00000	0.00672	0.00044	0.00525	-	2.53E-11	8.13E-15	29.9	2.13	71.219	0.025	**1521**	**5**
T01-19 bte grain 3.2	72.063	0.017	0.01306	0.00000	0.00236	-	-	-	1.46E-11	2.71E-15	47.1	0.00	72.063	0.017	**1533**	**5**
T01-19 bte grain 3.3	72.293	0.041	0.01383	0.00001	0.00565	-	0.00036	-	4.47E-11	2.44E-14	100.0	0.15	72.186	0.041	**1535**	**5**
T01-19 muscovite: J value = 0.018592 ± 0.000093																
T01-19 ms grain 1.1	22.058	0.014	0.01310	0.00003	0.10402	0.00041	0.00062	0.00001	1.20E-10	7.32E-14	66.6	0.83	21.875	0.014	**616**	**3**
T01-19 ms grain 1.2	21.905	0.014	0.01335	0.00005	0.28198	0.00122	0.00041	0.00005	2.55E-11	1.63E-14	80.7	0.55	21.785	0.021	**613**	**3**
T01-19 ms grain 1.3	22.530	0.016	0.01303	0.00015	0.06878	0.00163	-	-	2.01E-11	1.36E-14	91.9	0.00	22.575	0.016	**632**	**3**
T01-19 ms grain 1.4	24.216	0.020	0.01138	0.00021	0.11030	0.00528	0.00039	-	6.52E-12	3.03E-15	95.5	0.47	24.101	0.020	**668**	**3**
T01-19 ms grain 1.5	29.551	0.021	0.01256	0.00001	0.08003	0.00136	0.00099	-	8.02E-12	5.42E-15	100.0	0.99	29.257	0.020	**784**	**3**
T01-19 ms grain 2.1	18.663	0.008	0.01307	0.00004	0.00114	0.00000	0.00175	-	7.75E-11	3.25E-14	36.4	2.77	18.146	0.008	**524-1055)**	**2**
T01-19 ms grain 2.2	19.420	0.009	0.01275	0.00009	0.00188	0.00037	0.00304	-	2.94E-11	1.36E-14	50.2	4.63	18.522	0.009	**534**	**2**
T01-19 ms grain 2.3	19.124	0.006	0.01289	0.00005	0.00103	0.00000	0.00162	-	5.36E-11	1.08E-14	75.4	2.50	18.647	0.006	**537**	**2**
T01-19 ms grain 2.4	18.800	0.010	0.01250	0.00006	0.00323	0.00045	0.00062	0.00006	2.41E-11	1.08E-14	86.7	0.97	18.617	0.019	**536**	**2**
T01-19 ms grain 2.5	18.645	0.007	0.01245	0.00005	0.00157	0.00039	0.00034	0.00005	2.82E-11	5.42E-15	100.0	0.53	18.546	0.016	**534**	**2**
T01-24b biotite: J value = 0.018579 ± 0.000093																
T01-24b bte grain 1.1	266.982	0.299	0.01881	0.00002	0.01606	0.00002	0.00594	0.00001	7.29E-12	8.13E-15	16.9	0.66	265.225	0.297	**3208**	**8**
T01-24b bte grain 1.2	288.839	0.189	0.01481	0.00001	0.02204	0.00001	0.00254	-	8.50E-12	5.42E-15	36.5	0.26	288.087	0.188	**3333**	**8**
T01-24b bte grain 1.3	282.350	0.558	0.01518	0.00047	0.01845	0.02219	0.00189	0.00095	2.86E-12	5.59E-15	43.2	0.20	281.791	0.624	**3300**	**8**
T01-24b bte grain 1.4	287.861	0.191	0.01547	0.00010	0.01279	0.00477	0.00224	0.00020	1.33E-11	8.24E-15	73.9	0.23	287.199	0.200	**3329**	**8**
T01-24b bte grain 1.5	273.170	1.085	0.02196	0.00008	0.06136	0.01510	-	-	7.65E-13	2.71E-15	75.7	0.00	273.175	1.508	**3253**	**11**
T01-24b bte grain 1.6	284.985	0.152	0.01465	0.00001	0.01117	0.00155	0.00077	0.00036	1.05E-11	5.42E-15	100.0	0.08	284.757	0.186	**3316**	**8**
T01-24b bte grain 2.1	327.508	0.730	0.02053	0.00005	0.00861	0.01895	0.00298	0.00222	1.36E-12	3.03E-15	8.3	0.27	326.627	0.981	**3526**	**9**
T01-24b bte grain 2.2	361.214	0.379	0.01501	0.00050	0.00217	0.00478	0.00025	0.00025	5.41E-12	5.59E-15	41.2	0.02	361.140	0.387	**3683**	**8**
T01-24b bte grain 2.3	373.727	0.408	0.01231	0.00001	0.07049	0.00462	-	-	2.50E-12	2.71E-15	56.5	0.00	373.732	0.408	**3736**	**8**
T01-24b bte grain 2.4	371.301	0.568	0.01415	0.00002	0.00000	0.00000	-	-	1.78E-12	2.71E-15	67.3	0.00	371.301	0.568	**3726**	**8**
T01-24b bte grain 2.5	370.337	0.293	0.01455	0.00001	0.01020	0.00001	-	-	3.46E-12	2.71E-15	88.4	0.00	370.338	0.293	**3722**	**8**
T01-24b bte grain 2.6	371.699	1.586	0.01320	0.00006	0.00617	0.00003	-	-	1.91E-12	8.13E-15	100.0	0.00	371.700	1.586	**3728**	**10**
T01-24b muscovite: J value = 0.018566 ± 0.000093																
T01-24b ms grain 1.1	42.812	0.048	0.01276	0.00043	-	-	-	-	3.18E-12	2.71E-15	2.6	0.00	42.812	0.048	**1055**	**4**
T01-24b ms grain 1.2	33.229	0.012	0.01247	0.00004	0.00232	0.00015	0.00015	-	7.42E-11	2.44E-14	62.2	0.13	33.186	0.011	**866**	**3**
T01-24b ms grain 1.3	31.549	0.052	0.01085	0.00012	0.00702	0.00197	-	-	1.15E-11	1.90E-14	71.4	0.00	31.550	0.052	**832**	**4**
T01-24b ms grain 1.4	31.998	0.035	0.01221	0.00007	-	0.00000	-	-	2.00E-11	2.17E-14	87.6	0.00	31.998	0.035	**841**	**3**
T01-24b ms grain 1.5	30.421	0.015	0.01303	0.00018	0.00075	0.00073	-	-	1.55E-11	2.71E-15	100.0	0.00	30.421	0.054	**808**	**3**
T01-24b ms grain 2.1	41.721	0.040	0.01217	0.00001	0.01404	0.00279	0.00141	0.00047	5.75E-12	5.42E-15	20.8	1.00	41.304	0.145	**1027**	**5**
T01-24b ms grain 2.2	36.259	0.025	0.01251	0.00001	0.00836	0.00137	0.00033	0.00033	8.28E-12	5.42E-15	50.7	0.27	36.163	0.100	**927**	**4**
T01-24b ms grain 2.3	34.122	0.014	0.01283	0.00014	0.00594	0.00117	-	-	9.71E-12	3.03E-15	85.8	0.00	34.122	0.084	**885**	**4**
T01-24b ms grain 2.4	34.694	0.052	0.01387	0.00034	0.00587	0.00289	0.00069	0.00069	3.94E-12	5.59E-15	100.0	0.59	34.491	0.210	**893**	**6**

Reddy et al. JAES
Figure 1

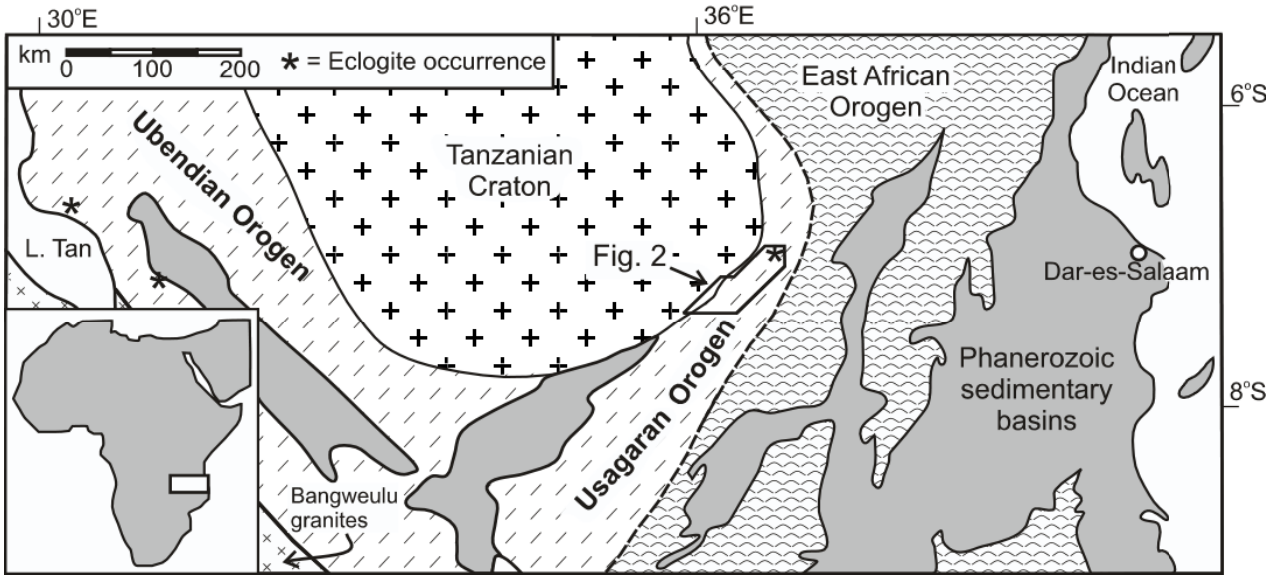

Reddy et al. JAES
Figure 2

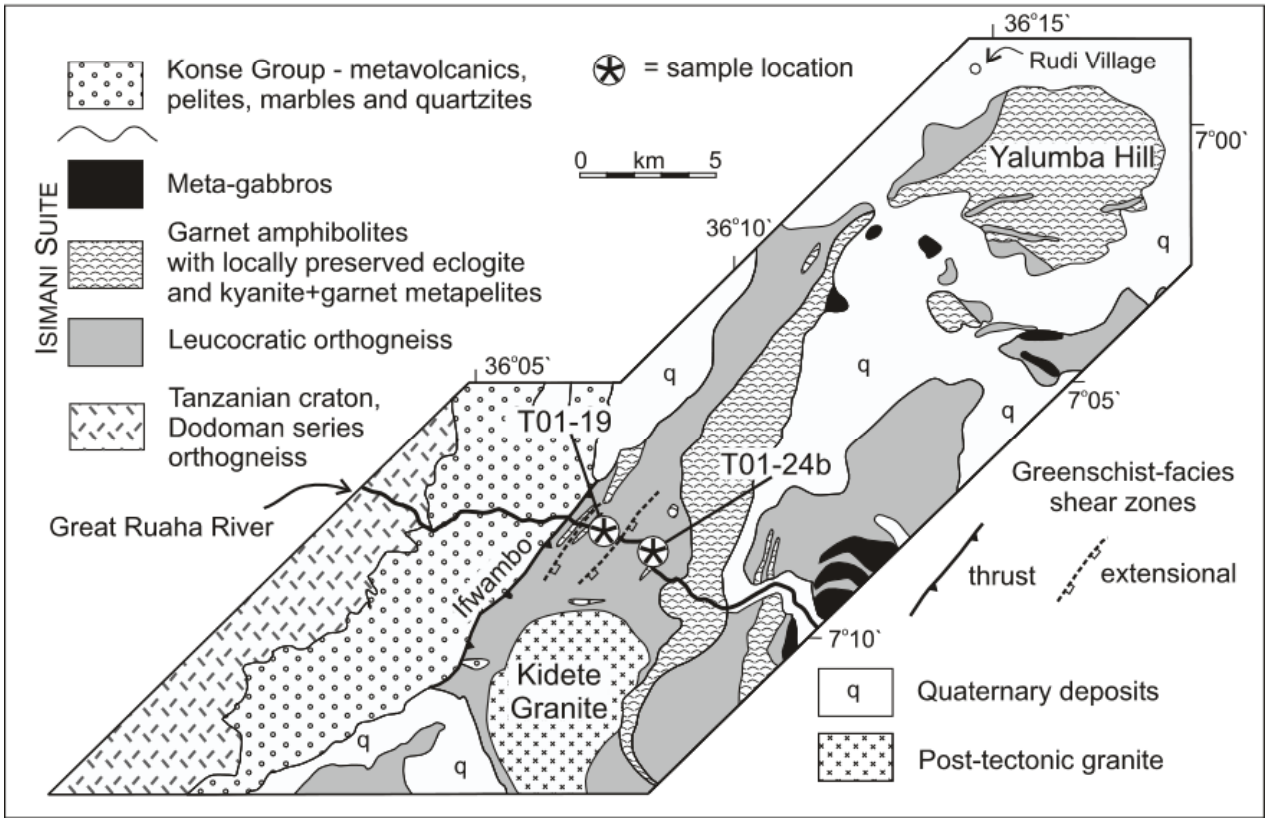

Reddy et al AJES
Figure 3

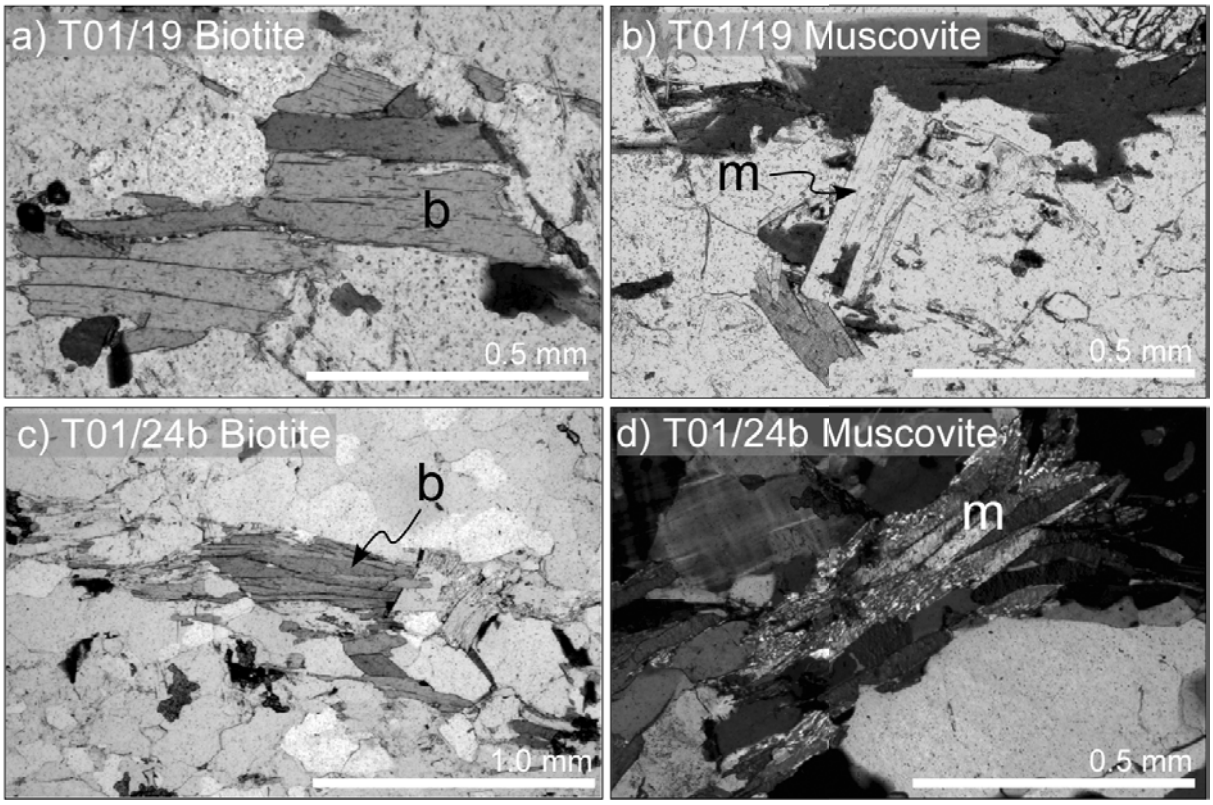

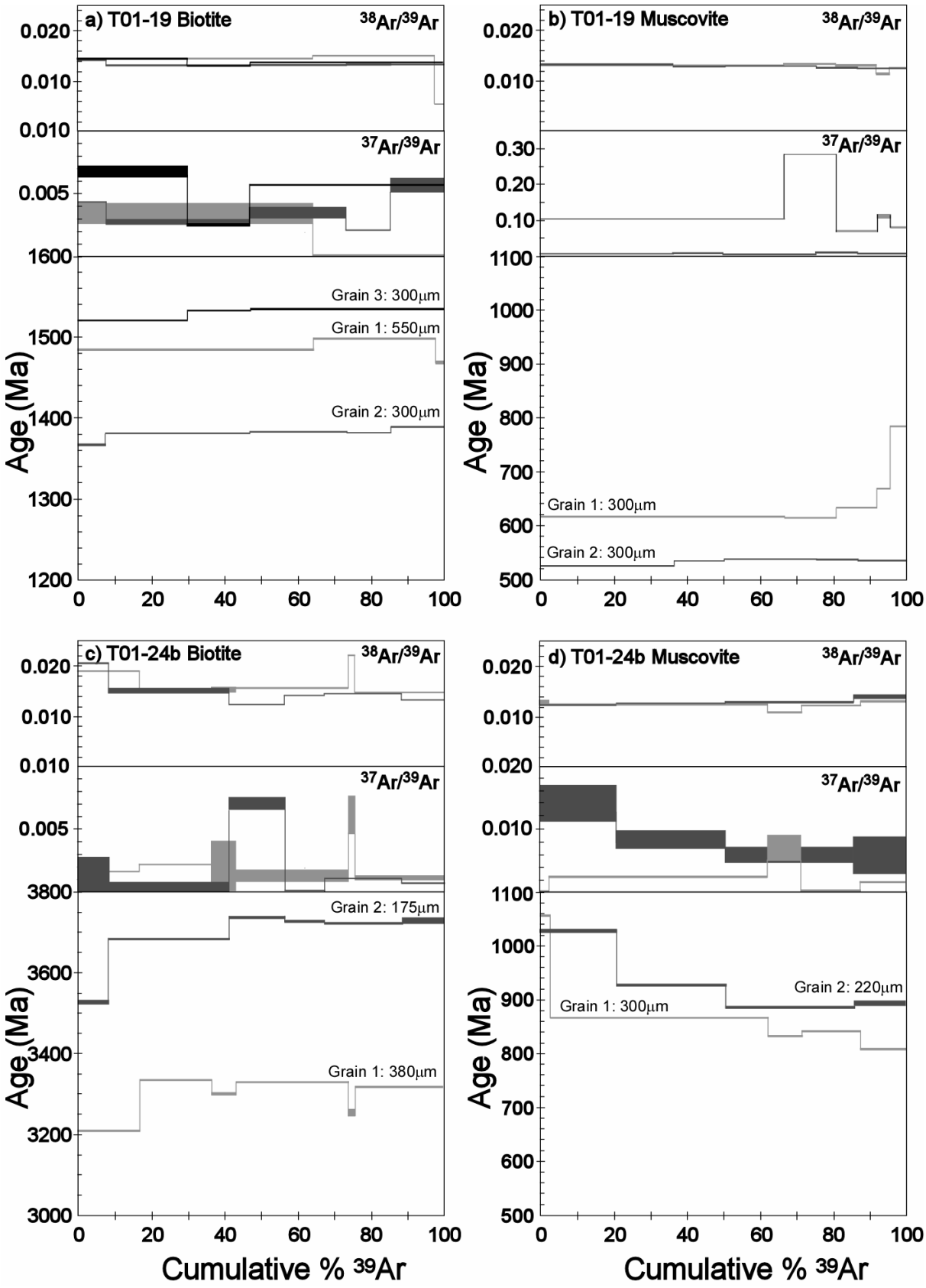

Reddy et al AJES: Figure 4